Stanford Exploration Project, Report 124, April 4, 2006, pages 49–66

Mapping of specularly-reflected multiples to image space: An example with 3D synthetic data

Gabriel Alvarez and Biondo Biondi

ABSTRACT

In 2D, specularly-reflected multiples, when migrated with the velocity of the primaries, map to negative subsurface offsets in Subsurface-Offset-Domain Common-Image Gathers (SODCIGs). In Angle-Domain Common-Image Gathers (ADCIGs) they map with curvature towards increasing depths. Here we show, through a 3D synthetic prestack dataset, that specularly-reflected multiples in 3D have a similar behavior with an interesting addition: in 3D ADCIGs, the multiples exhibit an azimuth rotation proportional to the dip of the reflecting interface generating the multiple. This attribute may be used to discriminate between primaries and multiples in 3D ADCIGs and therefore help in the attenuation of the multiples.

INTRODUCTION

In 2D, specularly-reflected multiples can be eliminated by Surface Related Multiple Elimination, SRME, (Verschuur et al., 1992; Berhout and Verschuur, 1997; Verschuur and Berkhout, 1997; Weglein et al., 1997; Dragoset and Jericevic, 1998) provided that there is no significant feathering, that short offsets can be acquired or accurately interpolated and that the subsurface is close to invariant in the crossline direction.

With 3D data, multiples are not only function of the inline offset but also of the crossline offset and thus SRME should be applied in 3D. In principle this is possible, since the theory of SRME is not limited to 2D data. In practice, however, the demands of SRME in terms of crossline sampling and crossline aperture make its application challenging. A great deal of research is being carried out on efficient and accurate ways of doing crossline interpolation and extrapolation and in making 3D-SRME practical from the computation point of view (van Dedem and Verschuur, 1998; Nekut, 1998), but this still remains a problem with most real datasets. An alternative, therefore, is needed for those cases where we are unable or unwilling to spend the human and computer resources necessary for 3D-SRME to work properly.

Given the relative simplicity of the Radon method applied in the image space (Alvarez and Artman, 2005), extending its application to account for the effect of crossline offset seems attractive. The first step in that direction is to understand how the moveout of the multiples

will behave on 3D Subsurface-Offset-Domain Common-Image Gathers (SODCIGs) and Angle Domain Common Image Gathers (ADCIGs). To that effect, we will use a very simple 3-D synthetic prestack dataset provided by ExxonMobil.

In the next section we describe the data in some detail to illustrate the difficulties of forming a complete dataset with uniform sampling in all five dimensions (time, inline and crossline position, and inline and crossline offset) small enough to fit in our computers. Then we briefly describe the preprocessing of the data and in the last two sections show the migration results of the primaries and multiples in pseudo and true 3D ADCIGs.

DESCRIPTION OF THE SYNTHETIC DATA

The velocity model used to generate the synthetic data is shown in Figure 1. The water bottom is deep, flat on the inline direction and dipping at 15 degrees in the crossline direction. The only reflector is a plane dipping 3 degrees in the inline direction and 15 degrees in the crossline direction.

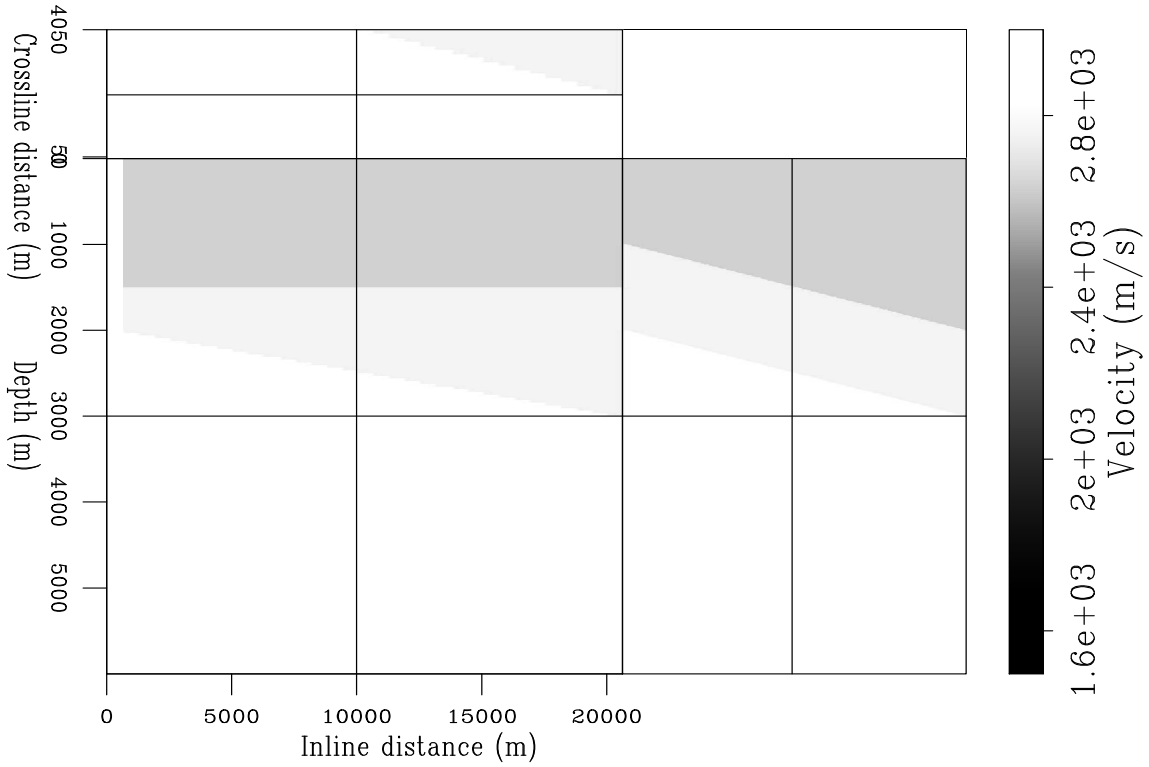

Figure 1: 3-D velocity model. gabriel2-model_vel [CR]

The geometry of acquisition consists of 10 receiver lines, each with 240 receivers spaced 25 m, with the first receiver at an inline offset of 100 m from the source. The maximum inline offset is therefore 6075 m. The receiver line separation is 100 m and the source is dual flip-flop with the two sources separated 50 m in the crossline direction and centered between the

two middle streamers with a 25 m crossline distance from the closest streamer. There are a total of 6 sail lines with each sail line separated from the next by a crossline distance of 450 m. With this arrangement, the crossline fold is just one and the fold in the inline direction is 60. Figure 2 shows a schematic of two adjacent sail lines illustrating that there is no overlap between the CMP coverage of each sail line. Figure 3 shows the receiver map, the source map, the azimuth-offset distribution and the fold map, all typical of a dual source flip-flop acquisition.

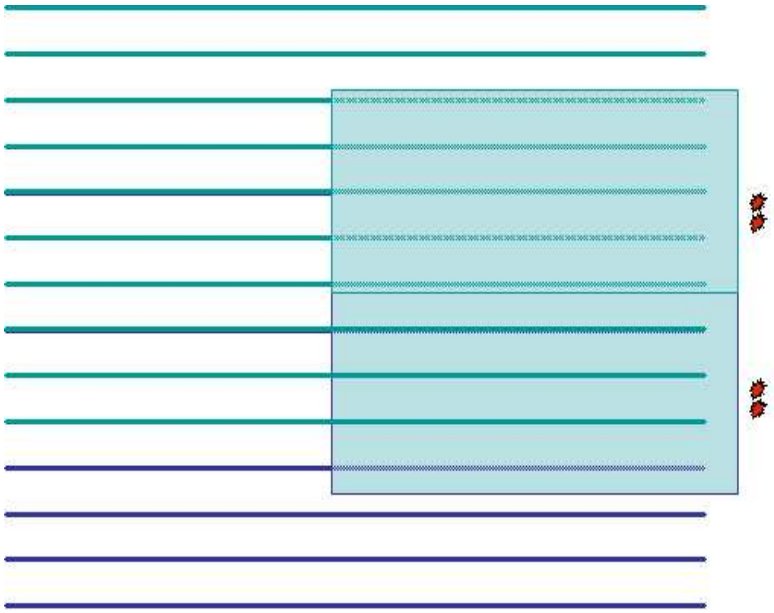

Figure 2: Schematic of fold coverage of two adjacent sail lines. gabriel2-sketch2 [NR]

Figure 4 shows a typical source record. The 10 receiver lines are clearly seen. There are four reflections: the water-bottom primary, the deeper reflector primary, the water-bottom multiple and the peg-leg reflection between the water-bottom and the deeper reflection. Notice the change in polarity of the multiples as compared to the primaries. Figure 5 shows a close up of the wavelet and the wavelet spectrum which shows that the wavelet has a DC component.

DATA SUBSET FOR S-R MIGRATION

The original dataset contains 6,764,207 traces (about 44 GB). Choosing a small, meaningful, "complete" subset of data for source-receiver migration, however, is not trivial, because the geometry of acquisition makes the offset distribution of adjacent CMPs in both inline and crossline directions different. This is illustrated in Figure 6 which shows the offset distribution inline for a few adjacent CMPs. Only every fourth CMP the offset distribution repeats. Although not shown, the situation in the crossline direction is worse. There are 20 different crossline offsets (from -475 to 475 m), but for any CMP line taken at a fixed crossline position, all traces correspond to the same crossline offset.

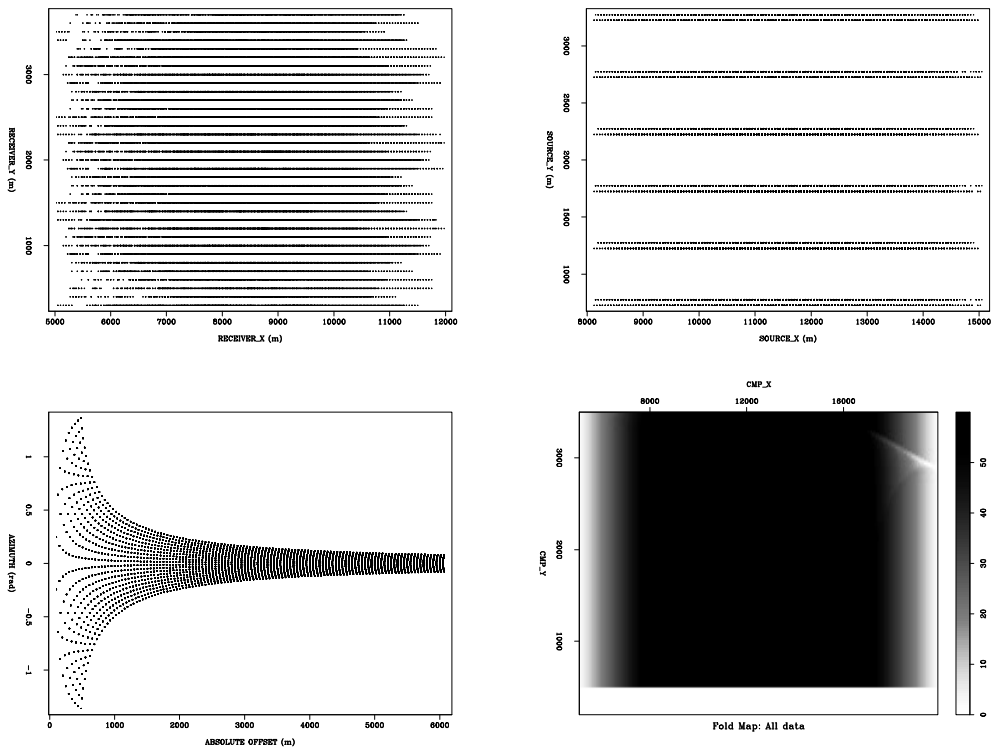

Figure 3: Top left: receiver map. Top right: source map. Bottom left: azimuth-offset distribution. Bottom right: fold map. gabriel2-attributes [CR]

The input to the source-receiver migration algorithm is a regular 5-D cube

$$D(t, \mathbf{m}, \mathbf{h}),$$

where $\mathbf{m}$ is the vector of surface position, $\mathbf{h}$ is the vector of surface offsets and t is the traveltime. In order to create such a cube, even for a small dataset, a large number of null traces need to be inserted. For example, for a 4 by 4 kms of full-fold CMP data we will have: 51200 CMPs (at 12.5 by 25 m) each with 240 inline offsets (100 to 6075 m offsets at 25 m sampling) and 20 crossline offsets (-475 to 475 m offsets at 25 m sampling) for a total of 440 million traces!. Since each trace has 1751 samples (7 seconds at 4 ms sampling interval), this means a dataset of almost 800 GB.

In order to make a more manageable dataset, further data reduction is necessary. Here we are particularly interested in the effect of crossline dip in the moveout of the multiples after migration, therefore we chose to subsample the data in the inline coordinates only. We subsampled the inline CMP axis such that every other CMP was discarded. This has the advantage of not only halving the number of CMPs but also halving the number of inline offsets as can be seen in Figure 6 since now the inline offset interval is 50 m rather than 25 m. We also subsampled the time axis to 16 ms, which required that the data be filtered to a maximum frequency of 32 Hz even though the original wavelet had frequencies up to about 60 Hz as shown in Figure 5. This is appropriate in this case because vertical resolution is not critical for our purposes. Finally, we limited the inline offsets to 4000 m which sacrifices the

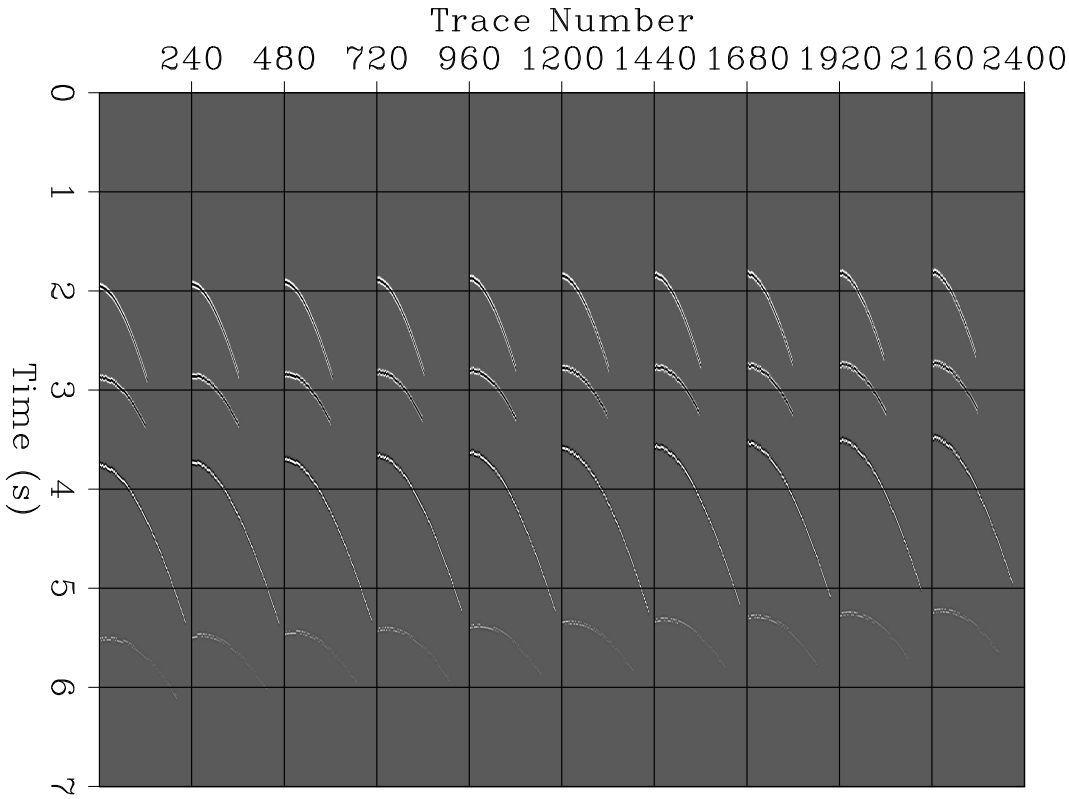

Figure 4: A typical "shot" gather showing the 10 receiver lines. Notice the polarity inversion of the multiples. gabriel2-shot [CR]

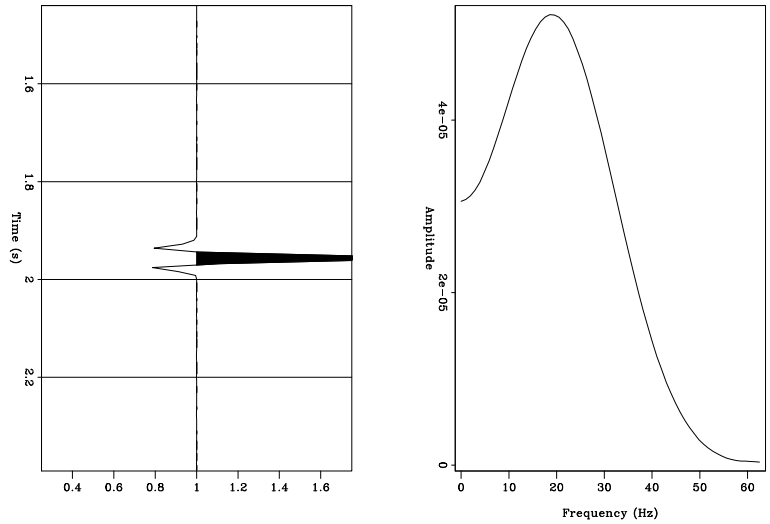

Figure 5: Close up of the seismic wavelet (a) and its frequency spectrum (b). Notice the uncharacteristic low frequencies. gabriel2-spectrum [CR]

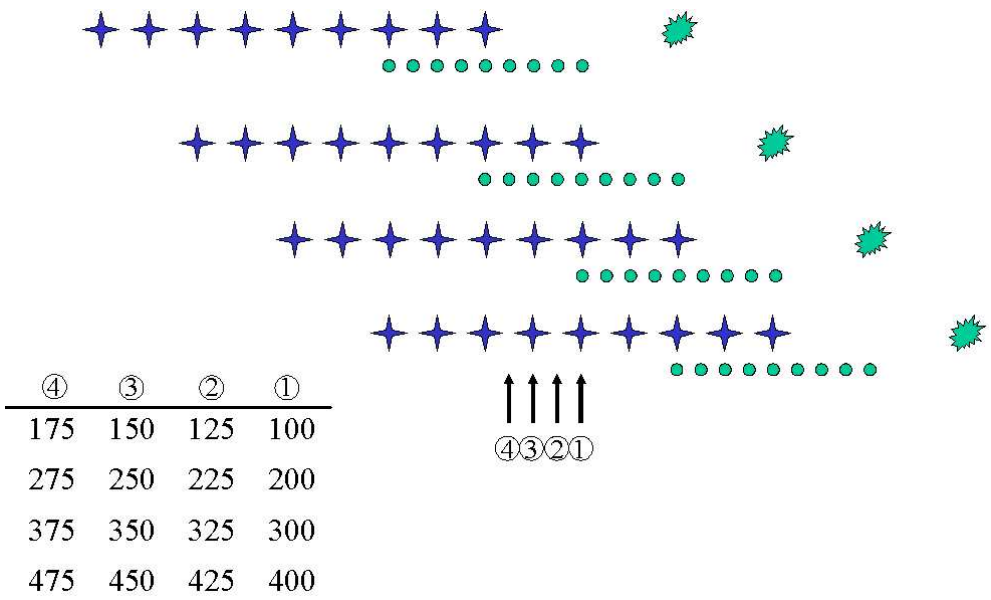

Figure 6: Schematic showing the unequal offset distribution of adjacent CMPs in the inline direction. The stars represent the receivers and the small circles represent the CMP positions. The table on bottom left side lists the offset distribution of a few traces corresponding to four arbitrary adjacent CMPs numbered 1 to 4 as indicated by the arrows. Notice that the adjacent CMPs have different offset distribution. gabriel2-sketch3 [NR]

steeper flanks of the moveout of the multiples as shown in Figure 4. With these reductions, the dataset size becomes about 70 GB after some padding in all spatial directions to avoid or at least lessen migration artifacts.

Figure 7 shows a near offset cube of the five-dimensional selected dataset. Notice that there are only six crossline CMPs for a given inline CMP location, corresponding to the six sail lines, and there is no data redundancy in the crossline direction. Similarly, only every other inline CMP position has a trace with a given crossline CMP location because of the dual shot geometry. Panel (a) of Figure 8 shows the inline and distribution of offsets for an inline CMP section taken at crossline CMP position 2212.5 and crossline offset of -12.5 m. Here again we note the on-off pattern of the offset distribution due to the dual shot source as indicated in the sketch in Figure 6. Similarly, panel (b) of Figure 8 shows the distribution of crossline offsets for a CMP section in the crossline direction taken at inline CMP location 8400 and inline offset of 100 m.

PREPROCESSING

Before attempting to do the full source-receiver migration on the data, we applied some pre-processing described briefly in this section.

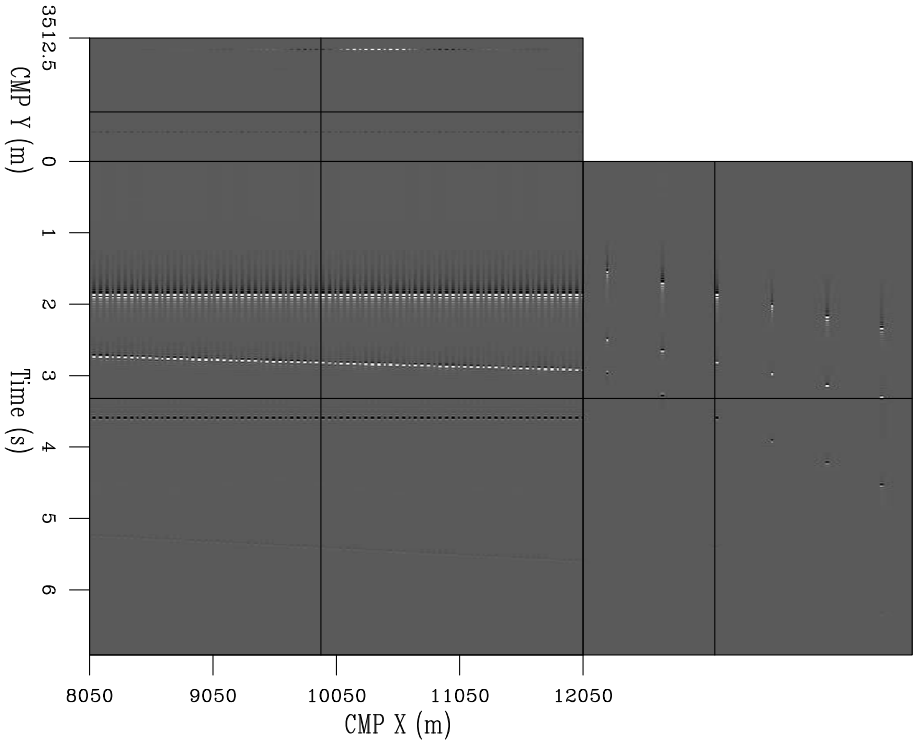

Figure 7: Near offset cube (50 m offset inline and -12.5 offset crossline) of the selected dataset. gabriel2-zoff1 [CR]

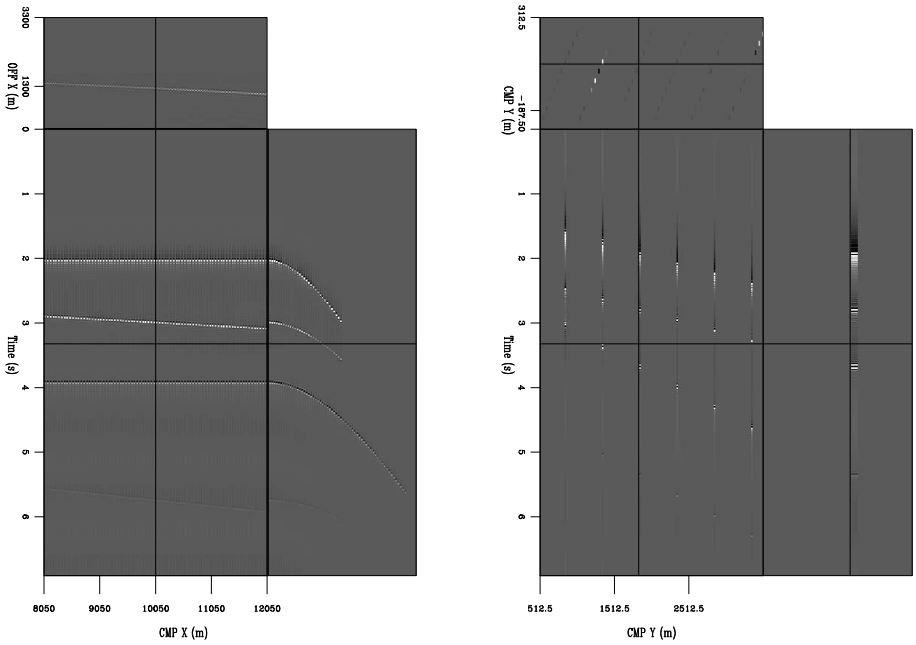

Figure 8: Left panel: inline distribution of offsets for an inline CMP section taken at crossline CMP location 2212.5 and at -12.5 m crossline offset. Right panel: crossline distribution of offsets for a crossline CMP section taken at inline CMP location 8400 and at 100 m inline offset. gabriel2-inline-xline [CR]

Data infill

The input data was first bandpass-filtered to remove the DC component and to limit the high frequencies to 32 Hz, and subsampled to 16 ms. It was then infilled with null traces in both offset dimensions, padded to add negative inline offsets and to extend the crossline aperture and sorted into a five dimensional regular cube of time, offset and CMP coordinates.

Datuming

The regular cube was then datumed to just above the water-bottom to avoid spending precious migration time on downward continuation through the water layer. Figure 9 shows a comparison of one CMP 3D gather before (left) and after datuming (right). Notice that datuming not only saves time but also allows a significant reduction of the data because the offsets decrease as the recording surface is "moved" closer to the reflectors, making the positions of sources and receivers closer. Notice also that the holes in both offsets and CMPs have been healed by the propagation.

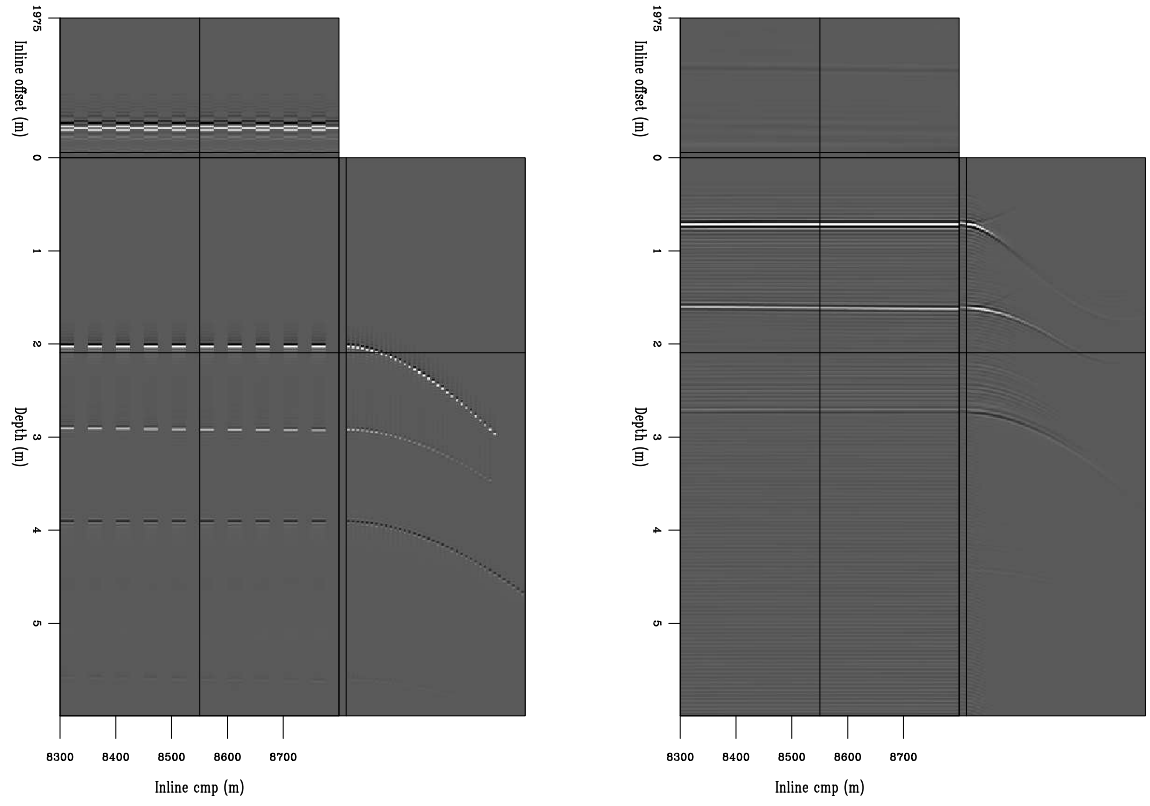

Figure 9: Comparison of a 3D CMP gather before (left) and after datuming (right). gabriel2-datum_comp [CR]

Common-Azimuth Migration

In order to choose the key migration parameters such as depth step, number of frequencies and especially padding of negative subsurface offsets to accommodate the migration of the multiples, we run some tests using common-azimuth migration. Rather than mapping the non-zero crossline offsets to zero cross-line offset via Azimuth Moveout, AMO, for compuitational simplicity we just windowed the nearest crossline offsets and assigned them to zero crossline offset.

Figure 10 shows the inline dimensions (CMP and offset) of an SODCIG after common-azimuth migration. Notice that the multiples have been mapped to the negative subsurface offsets and to shallower depths, consistent with the results obtained by Alvarez (2005). Figure 11 shows the zero subsurface offset cube which shows that the migrated image is good in the inline direction where the sampling was good but is poor in the crossline direction where the CMP sampling was coarse. Notice the multiple that was migrated with roughly twice the crossline dip and in the updip direction.

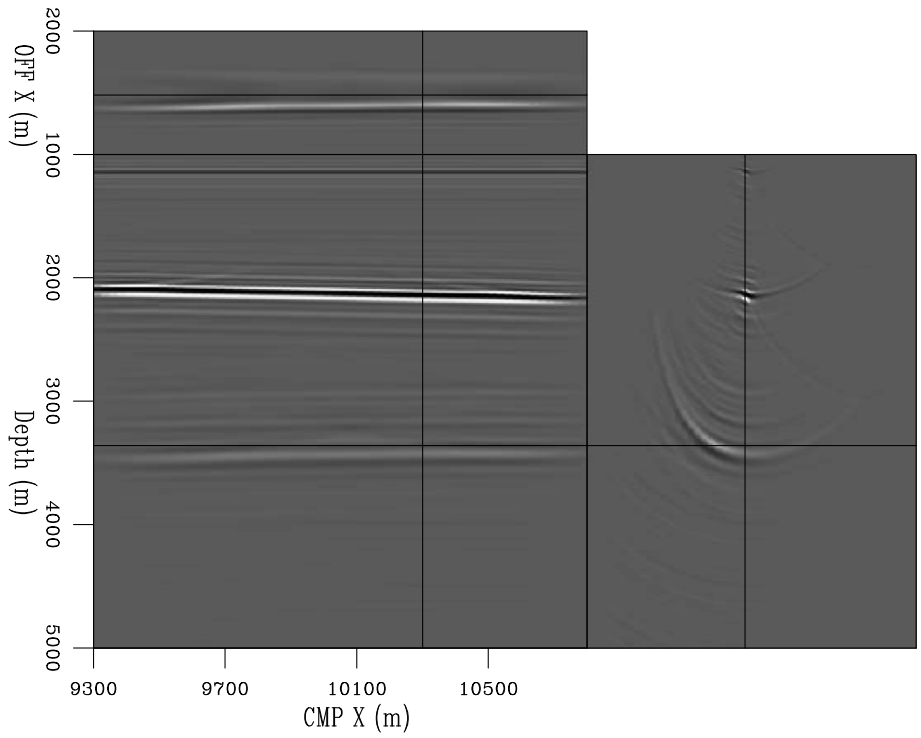

Figure 10: Inline SODCIG obtained by common-azimuth migration. gabriel2-cam1 [CR]

SOURCE-RECEIVER MIGRATION

After the data reduction afforded by the datuming and appropriate padding in offsets, we input to the source-receiver migration an even smaller dataset that had only 32 CMPs in the inline

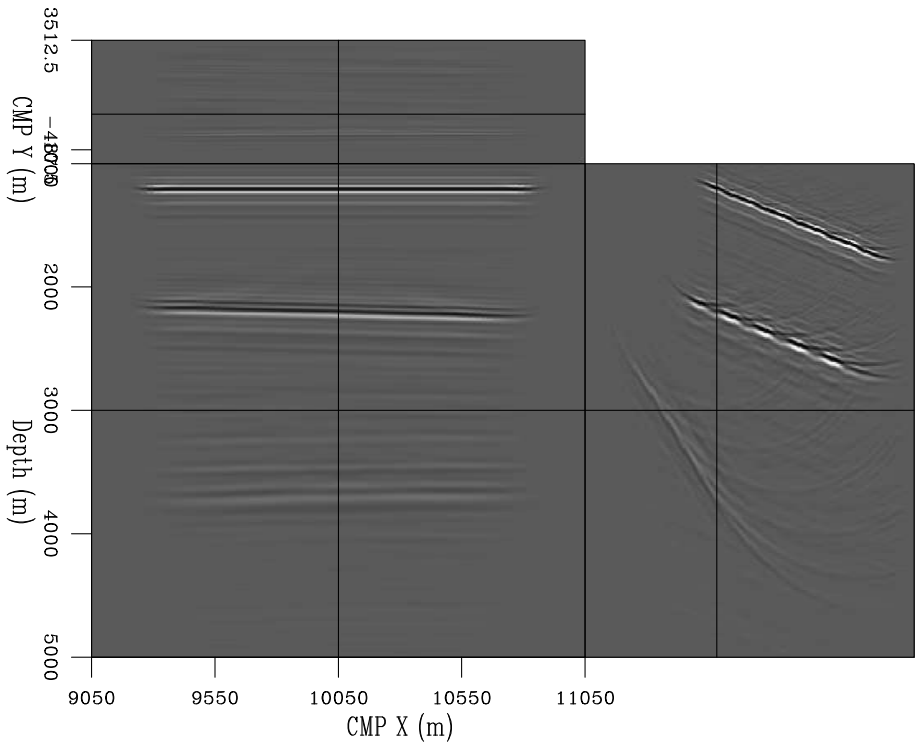

Figure 11: Zero subsurface-offset cube of data migrated with common azimuth migration. gabriel2-cam2 [CR]

direction, 144 CMPs in the crossline direction, 120 offsets in the inline direction, 24 offsets in the crossline direction and 200 frequencies, just about 20 Gb of data. The data was migrated with 600 depth steps at 10 m (starting at the depth of the water-bottom at zero crossline CMP or about 1000 m).

Figure 12 shows the inline dimensions of one SODCIG. The data aperture was very limited and so there are some migration artifacts. Again, note that the multiples migrate to the negative subsurface offsets and are well separated from the primaries.

By contrast with the inline direction, the sampling of the crossline offsets and CMPs is very coarse and the results of the migration are not nearly as good as illustrated in Figure 13 which shows a cube of crossline CMPs as a function of crossline offset. Although the primaries, and the multiple, have been relatively focused toward zero subsurface offset, there is still a lot of energy smearing to both positive and negative crossline subsurface offsets. Figure 14 shows a zero subsurface-offset cube of migrated data. The image is good in the inline direction and somewhat noisy in the crossline direction. A comparison with the result of the common-azimuth migration Figure 11 shows the improvement in the crossline image.

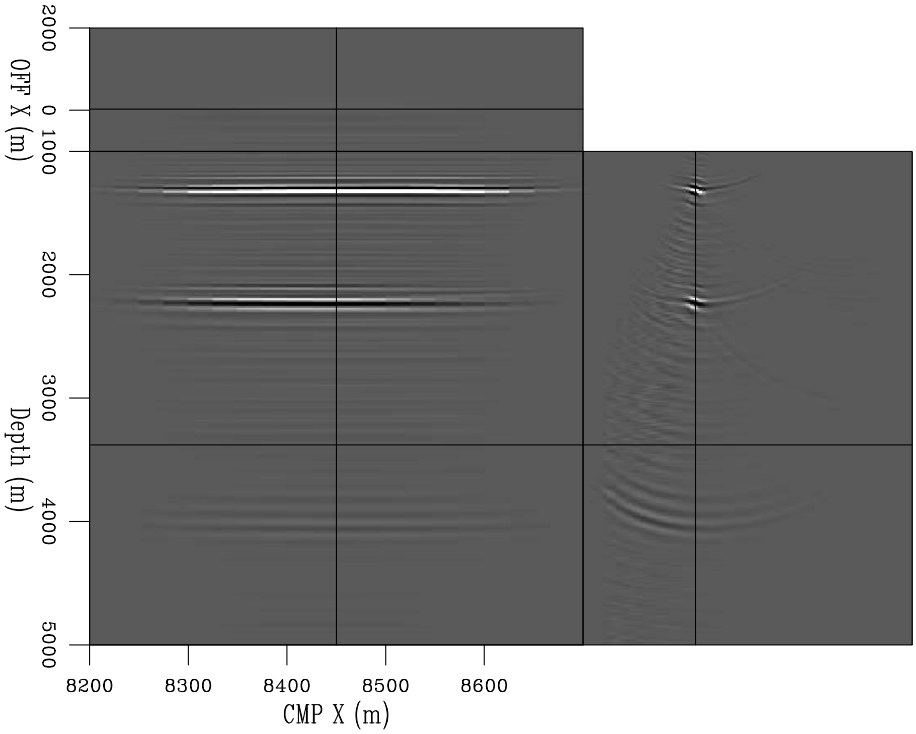

Figure 12: Inline SODCIG obtained by source-receiver migration. gabriel2-pre3dmig1 [CR]

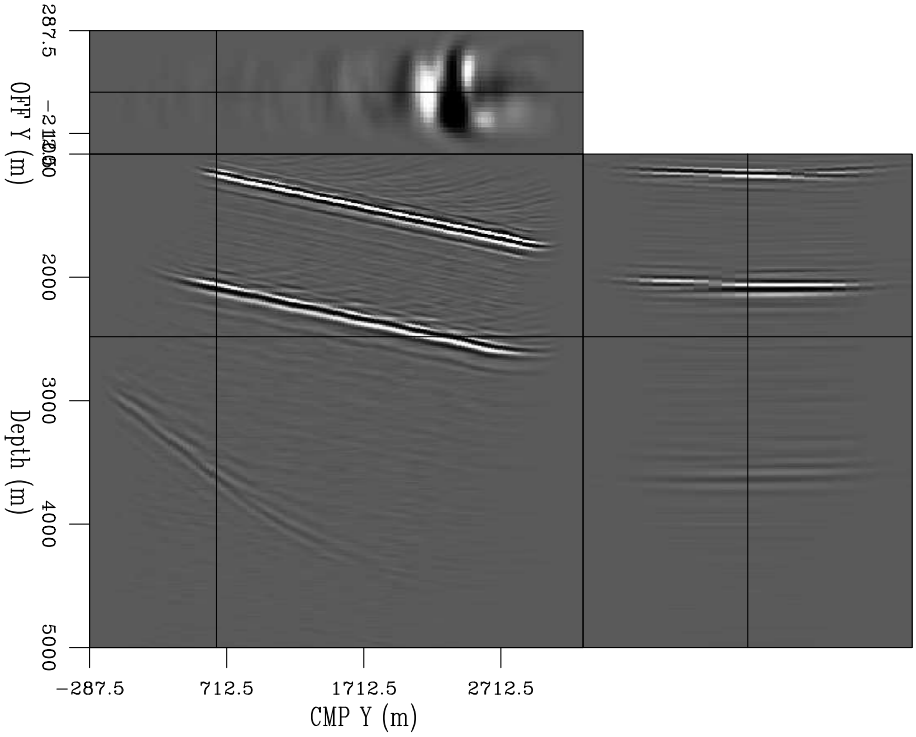

Figure 13: Crossline SODCIG obtained by source-receiver migration. gabriel2-pre3dmig3 [CR]

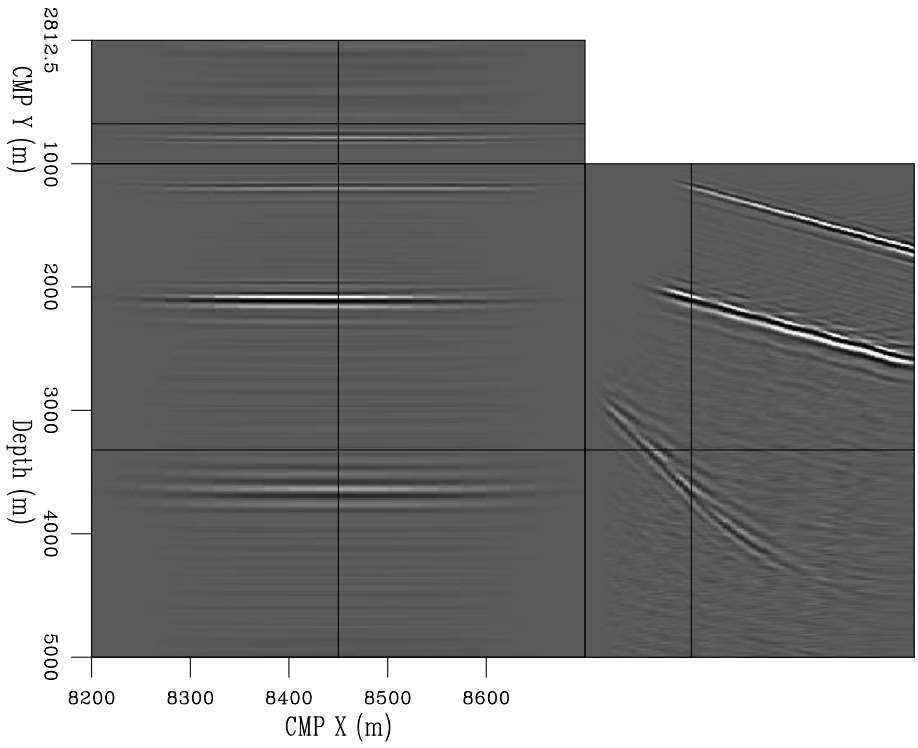

Figure 14: Zero subsurface-offset cube migrated with source-receiver migration. gabriel2-pre3dmig2 [CR]

TRANSFORMATION TO PSEUDO 3D ADCIGS

The basis for the computation of the 2D ADCIGs after migration is the equation

$$k_h = -k_z \tan\gamma, \tag{1}$$

(Sava and Fomel, 2003) where k_h and k_z are the offset and depth wavenumbers and γ is the aperture angle. In 3D the situation is more complicated because the azimuth of the reflection plane at the reflection point needs to be taken into account (Biondi, 2005) and the computation of true 3D ADCIGs as a function of the aperture angle and the azimuth of the reflection plane is not trivial (Biondi, 2005). We will explore this issue in the next section. It is tempting to compute pseudo-3D ADCIGs by a direct extension of equation 1, that is:

$$k_{h_x} = -k_z \tan\gamma_x \tag{2}$$
$$k_{h_y} = -k_z \tan\gamma_y \tag{3}$$

where x_{h_x} and k_{h_y} are the wavenumber components of the horizontal wavenumber vector and k_z, as before, is the depth component of the wavenumber vector. The angles γ_x and γ_y don't have an immediate correspondence with the aperture angle or the azimuth, hence we will call the ADCIGs obtained with equations 2 and 3 pseudo 3D ADCIGs. Panel (a) of Figure 15 shows the inline component of the pseudo ADCIG corresponding to the same SODCIG shown

in Figure 12. The primaries are flat and the multiples exhibit a similar residual moveout as that seen in 2D ADCIGs (Biondi and Symes, 2004). Panel (b) of Figure 15 shows the crossline component of the same pseudo 3D ADCIG. Since the crossline aperture is small, there is very little discrimination between the primaries and the multiples. This, of course means that using pseudo 3D ADCIGs to attenuate the multiples relies entirely on the inline direction and is therefore essentially a 2D process.

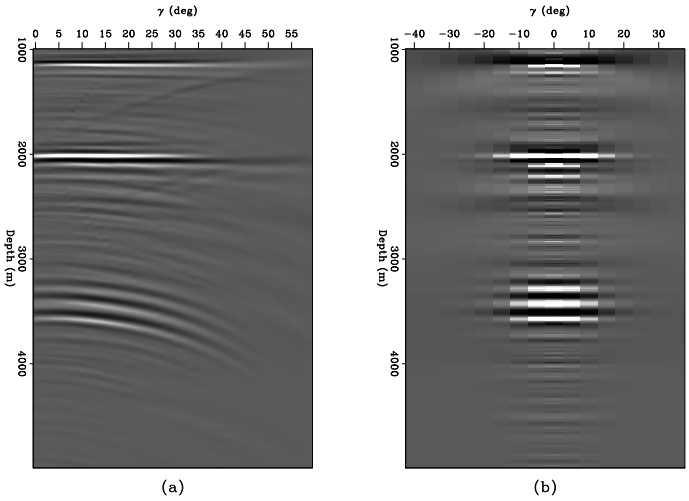

Figure 15: Inline component (a) and crossline component (b) of the pseudo 3D ADCIG corresponding to the SODCIG shown in Figure 12. gabriel2-adcigs [CR]

TRANSFORMATION TO TRUE 3D ADCIGS

The mathematical formalism and the methodology for computing true 3D ADCIGs as a function of the aperture angle γ and the data azimuth ϕ was given by Biondi and Tisserant (2004). They showed that the ADCIGs as a function of the aperture angle, for a fixed azimuth, may depart from flat even for migration using the correct velocity. As function of azimuth, the curvature of the events increase with increasing aperture angle. For a fixed depth, this translates into an azimuth rotation which depends on the dip of the reflector at that depth.

An important issue is to evaluate the degree of azimuth rotation difference between the water-bottom primary and the water-bottom multiple. Because of computational ease, we first windowed the SODCIGs in depth and computed the ADCIGs for the water-bottom primary only. Figure 16 shows the result for the same ADCIG as in Figure 15. It is flat for a given azimuth although the range of aperture angles is a function of the azimuth.

Similarly, we windowed the water-bottom multiple and computed the ADCIG as shown in Figure 17. The depth slice shows a small azimuth rotation when compared with the primary (compare the symmetry of the top panels of Figures 16 and 17). It is interesting to analyze the angle gathers as a function of azimuth for given aperture angles. The water-bottom primary and the water-bottom multiple behave very differently as shown in Figures 18 and 19. For the primary, as the aperture angle increases, the angle gather as a function of azimuth loses its flatness and curves down as shown in (Biondi, 2005). For the multiple, however, as the aperture angle increases the gather as a function of azimuth curves up because it is overmigrated.

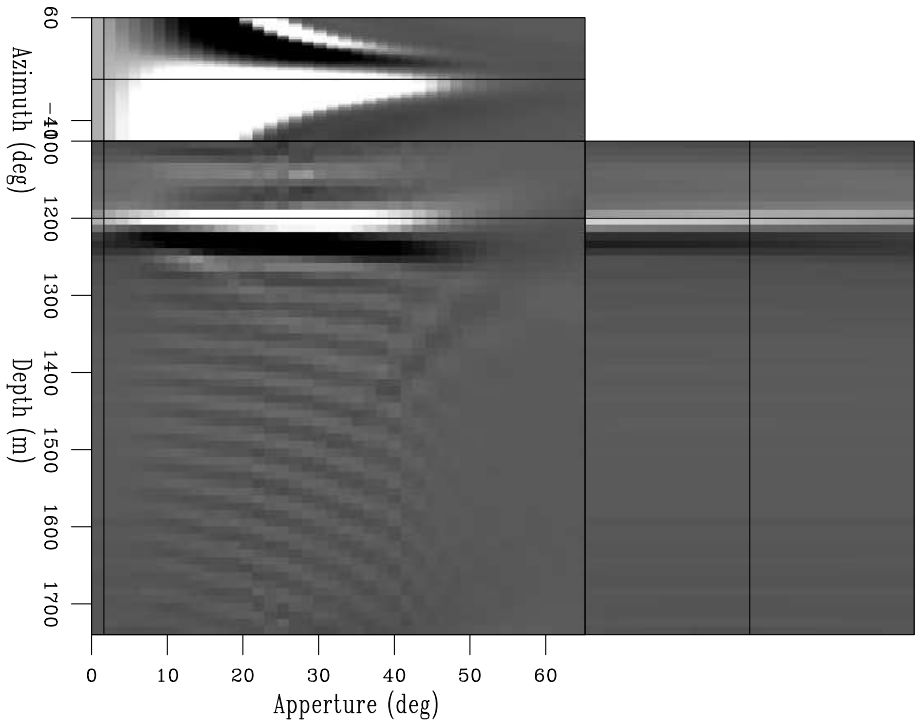

Figure 16: 3D ADCIG at a fixed spatial position for the water-bottom primary. gabriel2-3dadcig1 [CR]

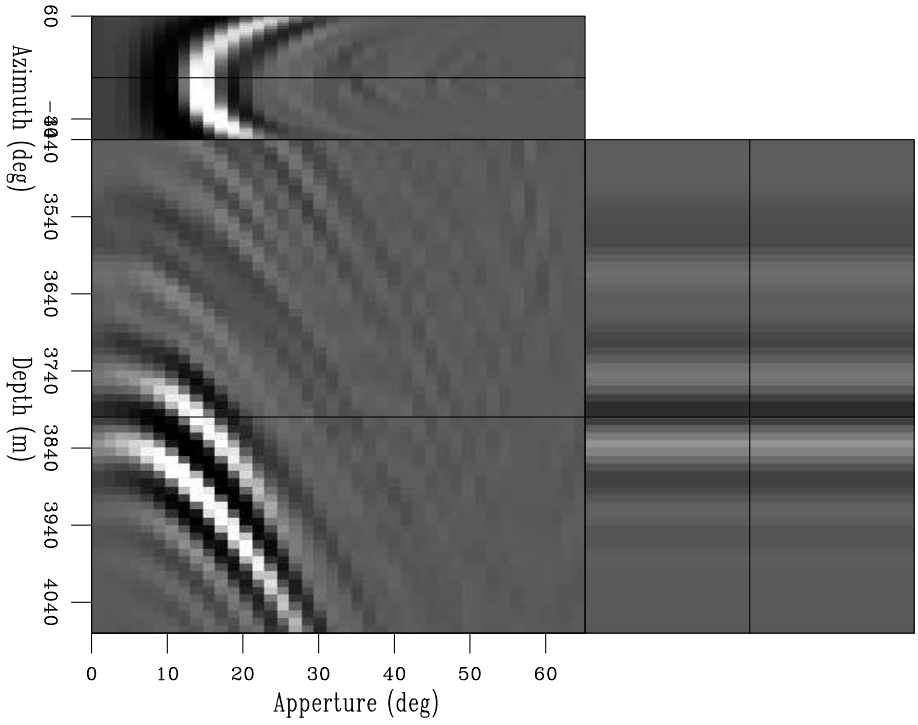

Figure 17: 3D ADCIG at a fixed spatial position for the water-bottom multiple. gabriel2-3dadcig2 [CR]

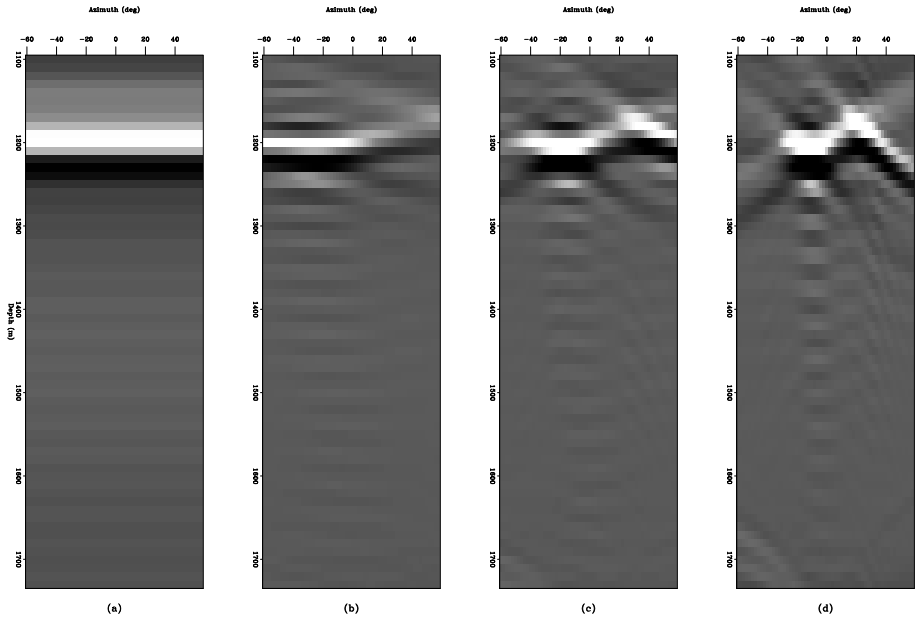

Figure 18: 3D ADCIG for the primary water-bottom reflection as a function of azimuth. The different panels correspond to different aperture angles: (a) 0, (b) 10, (c) 20 and (d) 30 degrees. gabriel2-az_gath1 [CR]

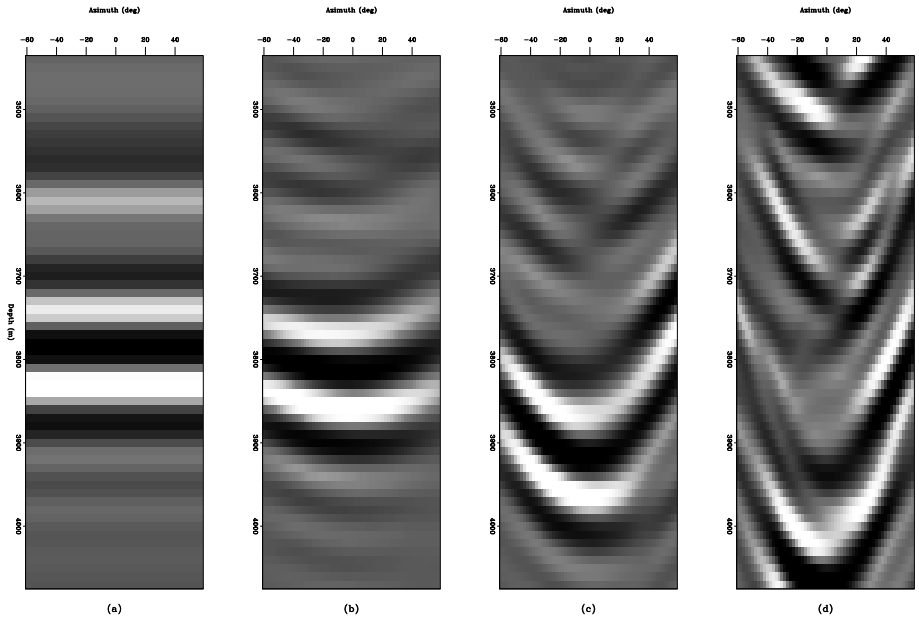

Figure 19: 3D ADCIG for the water-bottom multiple reflection as a function of azimuth. The different panels correspond to different aperture angles: (a) 0, (b) 10, (c) 20 and (d) 30 degrees. gabriel2-az_gath2 [CR]

DISCUSSION

The results of the previous sections show that primaries and multiples can be separated not only in ADCIGs but even in SODCIGs. In this case the crossline dips of the reflectors were relatively minor and little difference existed in the crossline component of the SODCIGs between the primaries and the multiples. Enough difference exists in the inline components, however, that a 2D style multiple attenuation can be carried out in the manner described by Alvarez (2006) in a companion paper in this report.

In addition, primaries and multiples can be discriminated on the basis of their residual moveouts in both pseudo as well as true 3D ADCIGs. In the first case, the discrimination is mostly in the inline component of the ADCIG since, as with the SODCIG not enough crossline dip exists in our dataset to provide a discrimination in the crossline component. Nonetheless, we can apply a Radon transform in the inline direction to separate the primaries and the multiples as done with 2D data (Sava and Guitton, 2003; Alvarez et al., 2004). In true 3D ADCIGs, there is the additional advantage of the multiples and the primaries behaving differently as a function of azimuth for a given aperture angle. This differential azimuth rotation may be exploited to compute a three-dimensional Radon transform that is a function of aperture angle and azimuth in a manner somewhat similar to the apex-shifted Radon transform used to attenuate 2D diffracted multiples (Alvarez et al., 2004). More research is needed to work out the implementation details, but the results of our tests are encouraging.

CONCLUSIONS AND FUTURE WORK

Although our tests were somewhat limited because the amount of data needed to form a complete five-dimensional dataset, even a very small area, strained our computer resources, they do show that even with 3D data we can discriminate between primaries and multiples in the image space. The practical details of the algorithms' implementations have not been worked out yet, but their relative simplicity is very attractive.

ACKNOWLEDGMENTS

We would like to thank ExxonMobil for providing the 3D synthetic dataset used in this paper.

REFERENCES

Alvarez, G. and B. Artman, 2005, Wavefield extrapolation in frequency-wavenumber domain for spatially-varying velocity models: SEP–**120**, 309–316.

Alvarez, G., B. Biondi, and A. Guitton, 2004, Attenuation of diffracted multiples in angle-domain common-image gathers:, *in* 74th Ann. Internat. Mtg. Soc. of Expl. Geophys., 1301–1304.

Alvarez, G., 2006, Attenuation of 2d specularly-reflected multiples in image space: SEP–**124**.

Berhout, A. and D. Verschuur, 1997, Estimation of multiple scattering by iterative inversion, part i: theoretical considerations: Geophysics, **62**, no. 5, 1586–1595.

Biondi, B. and W. Symes, 2004, Angle-domain common-image gathers for migration velocity analysis by wavefield-continuation imaging: Geophysics, **69**, no. 5, 1283–1298.

Biondi, B. and T. Tisserant, 2004, 3d angle-domain common-image gathers for migration velocity analysis: Geophysical Prospecting, **62**, 575–591.

Biondi, B., 2005, 3-D Seismic Imaging: http://sepwww.stanford.edu/sep/biondo/Lectures.

Dragoset, W. and Z. Jericevic, 1998, Some remarks on multiple attenuation: Geophysics, **63**, no. 2, 772–789.

Nekut, A., 1998, 3d surface-related multiple elimination: 68th Ann. Internat. Mtg., Soc. of Exp. Geophys., Expanded Abstracts, 1511–1514.

Sava, P. and S. Fomel, 2003, Angle-domain common-image gathers by wavefield continuation methods: Geophysics, **68**, 1065–1074.

Sava, P. and A. Guitton, 2003, Multiple attenuation in the image space: SEP–**113**, 31–44.

van Dedem, E. and D. Verschuur, 1998, 3d surface-related multiple elimination and interpolation: 68th Ann. Internat. Mtg., Soc. of Exp. Geophys., Expanded Abstracts, 1321–1324.

Verschuur, D. and A. Berkhout, 1997, Estimation of multiple scattering by iterative inversion, part ii: practical aspects and examples: Geophysics, **62**, no. 5, 1596–1611.

Verschuur, D., A. Berkhout, and C. Wapenaar, 1992, Adaptive surface-related multiple elimination: Geophysics, **57**, no. 9, 1166–1167.

Weglein, A., F. Gasparotto, P. Carvalho, and R. Stolt, 1997, An inverse scattering series method for attenuating multiples in seismic reflection data: Geophysics, **62**, 1975–1989.